Materials Science & Engineering A 695 (2017) 74–79

Contents lists available at ScienceDirect

Materials Science & Engineering A

journal homepage: www.elsevier.com/locate/msea

# Intrinsic properties and strengthening mechanism of monocrystalline Ni-containing ternary concentrated solid solutions☆

K. Jin[a], Y.F. Gao[a,b], H. Bei[a,*]

[a] Materials Science & Technology Division, Oak Ridge National Laboratory, Oak Ridge, TN 37831, USA
[b] Department of Materials Science & Engineering, University of Tennessee, Knoxville, TN 37996, USA

ARTICLE INFO

*Keywords:*
Solid solution alloys
Medium/high entropy alloys
Elastic constants
Nanoindentation
Solid solution strengthening

ABSTRACT

Ternary single-phase concentrated solid solution alloys (SP-CSAs), so-called "medium entropy alloys", not only possess notable mechanical and physical properties but also form a model system linking the relatively simple binary alloys to the complex high entropy alloys. The knowledge of their intrinsic properties is vital to understand the material behavior and to prompt future applications. To this end, three model alloys NiCoFe, NiCoCr, and NiFe-20Cr have been selected and grown as single crystals. Their elastic constants have been measured using an ultrasonic method, and several key materials properties, such as shear modulus, bulk modulus, elastic anisotropy, and Debye temperatures have been derived. Furthermore, nanoindentation tests have been performed on these three alloys together with Ni, NiCo and NiFe on their (100) surface, to investigate the strengthening mechanisms. NiCoCr has the highest hardness, NiFe, NiCoFe and NiFe-20Cr share a similar hardness that is apparently lower than NiCoCr; NiCo has the lowest hardness in the alloys, which is similar to elemental Ni. The Labusch-type solid solution model has been applied to interpret the nanoindentation data, with two approaches used to calculate the lattice mismatch. By adopting an interatomic spacing matrix method, the Labusch model can reasonably predict the hardening effects for the whole set of materials.

## 1. Introduction

The recent development of single-phase concentrated solid solution alloys (SP-CSAs), including high entropy alloys [1–4], has drawn great interest, because these alloys not only exhibit exceptional mechanical properties [5–7] and unique physical properties [8–11], but also provide intriguing new concepts for alloy development. Instead of modifying the microstructure with dilute solute species, the focus of developing those alloys is on the control of compositional complexity, i.e., the number, type, and concentration of alloying elements, while maintaining the alloys as single phase solid solutions [12]. While previous studies have shown that some of the material behaviors, e.g. sluggish diffusion, are correlated with the number of alloying elements [11], substantial experimental and theoretical evidence has shown that the type/combination of elements are more dominant in affecting their mechanical and physical properties. For example, the electrical resistivity of the ternary NiCoCr alloy is one order higher than that of another ternary NiCoFe alloy, even higher than the quaternary NiCoFeCr [8]. High electrical resistivity is attributed to the alloying of the Cr, which induces severe magnetic disorder due to the antiferromagnetic coupling of Cr atoms [8]. Regarding the mechanical properties, alloying Cr in Ni, Co, Fe, and Mn has shown very strong strengthening effects [13]. It is notable that some mechanical properties of ternary NiCoCr (e.g. strength, ductility and fracture toughness) are superior to those of the quaternary or even quinary NiCoFeCrMn alloys [6]. Recent studies have demonstrated that SP-CSAs can enhance irradiation resistance, making them promising in nuclear engineering applications [9]. Again, the combination rather than the number of elements plays the key role; for example the ternary alloy NiCoFe was reported to be more resistant to irradiation-induced swelling than the quaternary NiCoFeCr alloy [14,15].

Ternary SP-CSAs with equal or near equal atomic concentrations have been referred to as medium entropy alloys (MEAs) [6]. Besides extraordinary mechanical properties, some of them also possess unique physical properties, e.g., quantum critical behavior in NiCoCr alloy, which is surprising because such behavior usually appears in materials

☆ This manuscript has been authored by UT-Battelle, LLC under Contract No. DE-AC05-00OR22725 with the U.S. Department of Energy. The United States Government retains and the publisher, by accepting the article for publication, acknowledges that the United States Government retains a non-exclusive, paid-up, irrevocable, world-wide license to publish or reproduce the published form of this manuscript, or allow others to do so, for United States Government purposes. The Department of Energy will provide public access to these results of federally sponsored research in accordance with the DOE Public Access Plan (http://energy.gov/downloads/doe-public-access-plan).

* Corresponding author.
*E-mail addresses:* jink@ornl.gov (K. Jin), ygao7@utk.edu (Y.F. Gao), beih@ornl.gov (H. Bei).

http://dx.doi.org/10.1016/j.msea.2017.04.003
Received 21 February 2017; Received in revised form 31 March 2017; Accepted 2 April 2017
Available online 07 April 2017
0921-5093/ 

with very complex structure but the NiCoCr solid solution alloy has a simple face-centered cubic (FCC) crystal structure [10]. More importantly, the ternary SP-CSAs help bridge our existing knowledge on conventional (e.g. binary) alloys to the relatively less-understood complex high entropy alloys. In other words, these medium entropy alloys are an excellent model system to study the effect of alloying elements, since they limit the number of variables, but still have a relatively high degree of chemical complexity. Ni, Co, Fe, and Cr are among the most widely considered elements in the multi-component alloys according to a recent review of 408 alloys [16]. For example, a family of FCC SP-CSAs formed with these elements, from binary NiCo and NiFe to the quaternary NiCoFeCr, which are all subsets of the well-explored high entropy NiCoFeCrMn alloy, have been experimentally identified and their mechanical properties have been systematically studied [12,13,16]. Ni-Co-Cr, Ni-Co-Fe, as well as Ni-Fe-Cr are three possible FCC medium entropy alloy systems with these four elements. While single phase equiatomic NoCoFe and NiCoCr are available, the equiatomic NiFeCr does not form a stable single phase solid solution, instead second phases have been observed previously [12]. According to the isothermal section of the ternary Ni-Fe-Cr phase diagram at 627 °C (900 K) [17], the maximum Cr concentration for single-phase FCC solid solution is ~22 at%; therefore, a composition of NiFe-20Cr is selected and its single phase nature is subjected to be experimentally confirmed in this study.

The knowledge of intrinsic physical and mechanical properties is fundamental for comprehensive studies on material behavior and potential applications. Specifically, elastic constants are important to understand a broad range of material properties, including thermodynamic properties (e.g. Debye temperature), phonon properties, and defect (e.g. dislocation) behaviors. In this study, single crystalline NiFe-20Cr, NiCoFe and NiCoCr were grown, their elastic constants as well as lattice parameters, densities, and melting temperatures were measured, and several key material properties, e.g. shear moduli, bulk moduli, elastic anisotropy, and Debye temperatures were derived. The results obtained from the single-crystalline elastic constants are compared with the values directly measured from polycrystalline samples. Furthermore, nanoindentation tests were performed on these three alloys along with Ni, NiCo, and NiFe, to reveal their slip systems and to investigate the strengthening mechanisms. The strengthening in these alloys was interpreted by using the Labusch-type solid solution model with two different methods of calculating atomic mismatch. The success and limitation of these two methods are discussed.

## 2. Materials and experimental methods

### 2.1. Material preparation and single crystal growth

Pure Ni, Co, Fe, and Cr elemental metals (> 99.9% pure) of appropriate amounts were mixed by arc-melting. Each composition (arc-melted button) was flipped and re-melted five times before drop-casting the melt into a copper mold to ensure a homogeneous well-mixed alloy. The single crystals were grown from the polycrystalline as-cast ingots using a floating-zone directional solidification method. The details of single crystal growth can be found in Ref. [18] The single crystal rods were cut with two surface normal directions, < 100 > and < 110 > , in order to measure the elastic constants.

Previous studies [12] have demonstrated that equiatomic NiCoFe and NiCoCr can form stable FCC SP-CSAs. However, equiatomic NiFeCr alloy cannot form stable single phase solid solution alloys. We show here by slightly decreasing the concentration of Cr to 20 at%, the Ni-40Fe-20Cr does form a stable single-phase FCC solid solution. Fig. 1a shows a backscattered electron image of the microstructure of the as-cast NiFe-20Cr alloys, which consists of large elongated grains extending from the edges to the center, due to the heat flux during solidification. No secondary phase is observed in the microstructure images while its XRD pattern (not shown here) exhibits only FCC peaks. Furthermore, we have carefully characterized the composition distribution and microstructure after single crystal growth, and the single crystalline NiFe-20Cr is indeed a single-phase FCC solid solution. Figs. 1b and c show the patterns of X-ray backscatter Laue diffraction of NiFe-20Cr in surfaces oriented (100) and (110), respectively, which demonstrate good single crystal quality.

### 2.2. Material characterizations

The lattice parameters were measured by powder X-ray diffraction with Cu-target radiation at 40 kV and 40 mA on 2.54-mm thick slices. The samples were scanned through 2θ ranging from 20 to 90° with a scan rate of 1.2°/minute. The melting temperatures were determined using a NETZSCH 404 C differential scanning calorimeter (DSC). Here, the melting (solidus) temperature was defined as the start point at which the endothermic peaks were observed on the DSC traces upon heating from room temperature. The density, ρ, was measured using an AccuPyc 1330 pycnometer.

Nanoindentation tests were performed using a Nanoindenter XP with a Berkovich triangular pyramid indenter. Tests were conducted in the continuous stiffness mode (CSM) at room temperature at a constant $\dot{P}/P = 0.05\ s^{-1}$, to a maximum load of 20 mN for hardness measurements. The nanoindentations to a maximum load of 100 mN were also performed to obtain clear slip trace patterns which were imaged using a Nikon Epiphot 300 optical microscope.

For single crystals, the elastic constants $c_{11}$, $c_{12}$ and $c_{44}$, were determined by measuring the longitudinal and transverse sound wave velocities ($V_l$ and $V_t$) inside the materials along < 100 > and < 110 > directions, based on the following equations [19].

Along < 100 > ,

$$V_l = \sqrt{\frac{c_{11}}{\rho}}, \tag{1}$$

$$V_t = \sqrt{\frac{c_{44}}{\rho}}. \tag{2}$$

Along < 110 > ,

$$V_l = \sqrt{\frac{c_{11} + c_{12} + 2c_{44}}{2\rho}}. \tag{3}$$

The effective polycrystalline elastic properties such as shear modulus and Poisson's ratio were calculated using both the Voigt-Reuss ($G_V$-$G_R$) and Hashin-Shtrikman ($G_H$-$G_S$) models, as described in detail in Refs. [20] and [21].

The elastic properties were also measured directly on polycrystalline samples. To do this, the as-cast alloy was first compressed by ~60%, and then annealed at 900 °C for 3 h to produce a fully recrystallized microstructure. In the polycrystalline case [22], the shear modulus and the Poisson's ratio were determined using

$$G = V_t^2 \rho \tag{4}$$

and

$$\upsilon = \frac{1 - 2(V_t/V_l)^2}{2 - 2(V_t/V_l)^2}. \tag{5}$$

## 3. Results

### 3.1. Intrinsic physical properties and elastic constants

The lattice parameter, density and melting temperature of NiFe-20Cr are listed in Table 1; the values of NiCoCr and NiCoFe [13,23] are also shown for comparison. The lattice parameter of NiFe-20Cr is greater than that of both NiCoFe and NiCoCr, probably because the Fe and Cr have larger atomic size than Co [24]. This is similar to the case of binary alloys, in which the lattice parameter of FCC Ni-xFe and Ni-

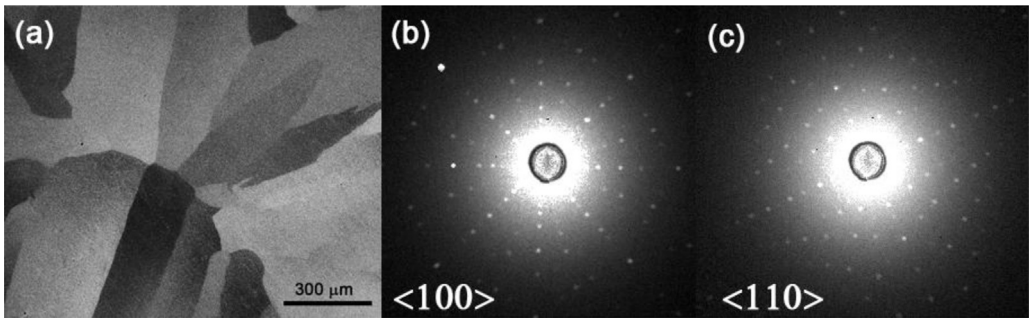


**Fig. 1.** (a) Backscattered electron image of as-cast NiFe-20Cr. (b) and (c) Backscattered X-ray Laue diffraction patterns of single-crystalline NiFe-20Cr with surface normal close to < 100 > and < 110 > , respectively.

**Table 1**
Fundamental physical properties and elastic properties of NiCoFe, NiCoCr and NiFe-20Cr.

| | NiFe-20Cr | NiCoFe | NiCoCr |
|---|---|---|---|
| a (Å) | 3.582 | 3.569 [23] | 3.559 [23] |
| Density (g $cm^{-3}$) | 8.126 | 8.390 [23] | 8.273 [23] |
| $T_m$ (K) | 1686 | 1724 [12] | 1690 [12] |
| $V_l$ [100]/[110] (m/s) | 5112/6057 | 5052/5982 | 5486/6455 |
| $V_t$ [100] (m/s) | 3862 | 3686 | 4144 |
| $C_{11}$ (GPa) | 212 | 214 | 249 |
| $C_{12}$ (GPa) | 142 | 159 | 156 |
| $C_{44}$ (GPa) | 121 | 114 | 142 |
| $G_{V\text{-}R}$ [$G_V$/$G_R$] (GPa) | 74 [87/62] | 65 [80/51] | 91 [104/78] |
| $G_{H\text{-}S}$ [$G_H$/$G_S$] (GPa) | 75 [78/71] | 66 [70/61] | 91 [94/88] |
| K (GPa) | 165 | 177 | 187 |
| υ | 0.31 | 0.34 | 0.29 |
| E (GPa) | 194 | 174 | 234 |
| A | 3.4 | 4.1 | 3.1 |
| $V_m$ (m/s) | 3378 | 3128 | 3694 |
| $\Theta_D$ (K) | 448 | 415 | 490 |

xCr alloys are greater than that of Ni-xCo alloys [25,26]. The density of NiFe-20Cr is lower than the other two alloys, while their melting temperatures are similar.

The elastic constants $c_{11}$, $c_{12}$ and $c_{44}$, calculated using Eqs. (1)–(3) are listed in Table 1. The bulk modulus is calculated as $(c_{11}+2c_{12})/3$; the upper and lower bounds and the average of effective shear modulus, calculated using Voigt-Reuss model ($G_{VR}$) and Hashin-Shtrikman model ($G_{HS}$), are also presented. As expected, the average values using these two calculation methods are similar, while the H-S model gives a narrower range. Accordingly, the Poisson's ratio and Young's modulus are then derived based on the H-S model. The shear modulus and Poisson's ratio directly from the measurements on polycrystalline samples are listed in Table 2. The Poisson's ratios derived from the single crystalline elastic constants are very similar to those measured from polycrystalline samples, while the shear moduli obtained from these two methods deviate slightly - up to ~6%. These differences, other than the contribution from experimental uncertainties, might be attributed to the textures in the polycrystalline samples, especially for those alloys having large elastic anisotropy, defined as $A=(2c_{44})/(c_{11}-c_{12})$, as shown in Table 1.

Teklu et al. [27] reported the elastic constants of Fe-15Ni-15Cr and compared them with a series of Fe-Ni-Cr alloys with Ni concentration within 8–24 at% and Cr concentration within 12–19 at%, and they found that the elastic constants have very little dependence on the Ni concentration, which is consistent with the present study, since all the elastic constants of NiFe-20Cr, including the anisotropy are similar to those for Fe-18, 19Cr-xNi, for x within 12–25 at%. In fact, the elastic constants of Ni-40Fe-20Cr are also similar with those of Fe-12Cr-12Ni, in which the $c_{11}$, $c_{12}$, and $c_{44}$ are 211, 140, and 123 GPa, respectively, which further suggests that the elastic properties of Ni-Fe-Cr system are not very sensitive to the composition within the FCC phase when the concentration of Cr is greater than 12 at%.

Debye temperature is one of the most important solid-state dynamic parameters that can be derived from elastic constants. Here the Debye temperature$\Theta_D$ of the three ternary alloys have been derived [27] from a standard equation

$$\Theta_D = \left(\frac{h}{k_B}\right)\left(\frac{3}{4\pi V_a}\right)^{1/3} V_m, \tag{6}$$

where $h$ is the Planck's constant, $k_B$ is Boltzmann's constants, $V_a$ is atomic volume. $V_m$ is the mean sound velocity, which is:

$$V_m = \left[\frac{1}{3}\left(\frac{2}{<V_t>^3} + \frac{1}{<V_l>^3}\right)\right]^{-1/3}, \tag{7}$$

where $< V_t >$ and $< V_l >$ are the average sound velocities, determined from the single crystalline elastic constants based on the Voigt-Reuss-Hill-Gilvary approximations. Details of the calculation and justifications were proposed by Anderson [28]. For NiFe-20Cr, the derived $V_m$, 3378 m/s (see Table 1), is close to that obtained from a polycrystalline sample, 3494 m/s, despite the possible errors from the structural anisotropy as discussed above. The derived Debye temperature values of NiFe-20Cr, NiCoFe and NiCoCr are 448, 415 and 490 K, respectively, which are similar to the literature value of 451 K for Fe-15Ni-15Cr [27].

**Table 2**
Single crystal nanoindentation hardness [at (100) surface], polycrystalline shear modulus and Poisson's ratio of NiFe-20Cr, NiCoFe, NiCoCr, NiFe, NiCo and Ni. The values of Fe-30Ni and Fe-15Ni-15Cr from Ref. [19] are also listed. The G and ν values of the alloys other than NiFe-20Cr are from the Refs. [19] and [23].

| | H (GPa) | G (GPa) | υ |
|---|---|---|---|
| NiFe-20Cr | 1.91 ± 0.09 | 80 | 0.29 |
| NiCoFe | 1.82 ± 0.03 | 60 | 0.35 |
| NiCoCr | 2.74 ± 0.1 | 87 | 0.30 |
| NiCo | 1.31 ± 0.02 | 84 | 0.29 |
| NiFe | 1.96 ± 0.04 | 61 | 0.34 |
| Ni | 1.18 ± 0.04 | 76 | 0.31 |
| Fe-30Ni [19] | 1.43 ± 0.02 | 65 | – |
| Fe-15Ni-15Cr [19] | 1.46 ± 0.02 | 79 | – |

### 3.2. Slip trace analysis

Fig. 2 shows the slip trace pattern of NiFe-20Cr on its (100) surface after nanoindentation to the maximum load of 100 mN, and that of the other alloys (NiCo, NiFe, NiCoFe, and NiCoCr) are shown in the Supplementary material. A typical square-like slip trace pattern can be clearly identified when a three-sided pyramidal indenter is used. In FCC metals, because of the crystallographic symmetry, both (111) and (11-1) slip planes intersect the (001) surface along the [1-10] directions, and both the (-111) and (1-11) slip planes intersect the (001) surface along the [110] direction, resulting in the square-like pattern on the (100) surface [19]. Two sets of parallel lines occur in the slip steps, and each {111} plane has the same intersection angle with respect to

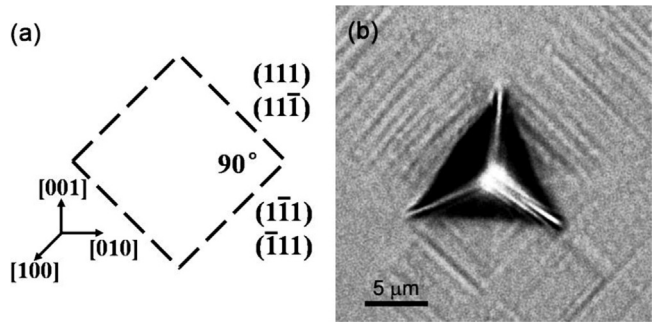


**Fig. 2.** (a) Predicted slip traces in (100) oriented surface of a FCC single crystal. (b) The observed slip traces on the (100) surface of NiFe-20Cr after nanoindentation to a load of 100 mN.

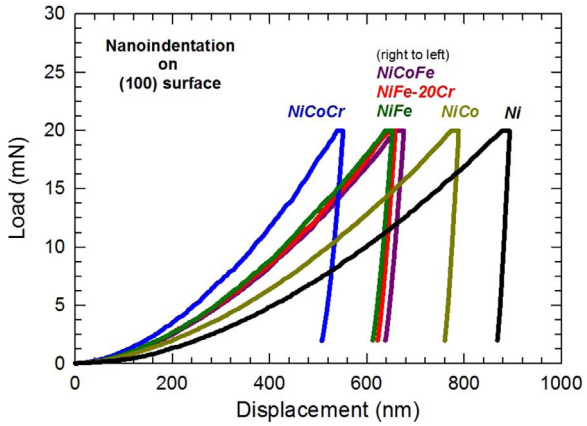


**Fig. 3.** Load-displacement curves of NiCoCr, NiCoFe, NiFe-20Cr, NiFe, NiCo, and Ni, to a maximum load of 20 mN.

the [100] direction. All the tested alloys display typical FCC slip traces after indentation.

### 3.3. Nanoindentation hardness

The load-displacement curves of all these alloys are plotted together in Fig. 3, and the corresponding hardness is listed in Table 2. These alloys are divided into three groups: (1) NiCo, which has a similar hardness to pure Ni, (2) NiFe, NiCoFe and NiFe-20Cr, which have similar moderately increased hardnesses, and (3) NiCoCr, which has much higher hardness than the others.

It is expected that the addition of Cr has significant strengthening effects in Ni-based SP-CSAs [13], due to the large modulus mismatch (the shear moduli of Ni, Co, Fe and Cr are 76, 75, 82, and 115 GPa, respectively [29]). However, interestingly, although NiCoCr has a much higher hardness than NiCo, which could be explained by the modulus mismatch, the hardness of NiFe-20Cr is not higher than NiFe. In fact, Xia et al. [19] have found that, comparing FCC Fe-30Ni and Fe-15Ni-15Cr, although their elastic constants have large differences, their indentation hardnesses are almost the same (see Table 2). Both results show that addition of Cr in the FCC NiFe- system is far less efficient in strengthening, compared with that in the NiCo-system.

## 4. Discussion

The strengthening mechanism of SP-CSAs has attracted much interest, and several models have been proposed or applied, among which the model proposed by Labusch [30] originally for binary alloys has been adopted and modified to explain the strengthening in multi-component alloys, or even high entropy alloys [31,32]. According to the Labusch model, the additional strength from the solid solution hardening is given by

$$\Delta\sigma_{solute-strengthening} = fG\left\{\sum_i x_i\left[\left(\frac{\eta_i}{1+\frac{1}{2}|\eta_i|}\right)^2 + \alpha^2\delta_i^2\right]\right\}^{2/3}, \quad (8)$$

where $f$ is a dimensionless parameter, $G$ is the shear modulus, $\delta$ describes the lattice mismatch, $\eta$ describes the modulus mismatch, $x_i$ is the concentration of element $i$, and $\alpha$ is a dimensionless parameter that describes the type of dislocations, which is ~3–16 for screw dislocations, and > 16 for edge dislocations.

The lattice and modulus mismatch between different alloying elements are two key parameters in this model, while the way of calculating these parameters varies in different studies. For example, Toda-Caraballo et al. [32] adopted an "interatomic spacing matrix (ISM)", initially proposed by Moreen [33], to calculate the average distance between each pair of elements i and j, based on the values of lattice parameter and bulk modulus of the pure i and j metals in their respective crystal structure, the atomic fraction of each element, and an empirical translating factor between different crystal structures. Wu et al. [31] in contrast, applied an alternative practical treatment, so-called pseudo-inverse analysis (PIA), for those non-FCC elements, e.g. Fe, Co, Cr and Mn, assumed Vegard's law valid for the lattice parameter of the target alloy systems (e.g. NiCo, NiCoFe etc.), and then derived the effective atomic size of each element in FCC structures based on the experimental lattice parameters of the selected alloys by solving a set of linear equations. Moreover, Wu et al. considered the $\alpha$ values from 0 to 20, while Toda-Caraballo et al. assumed a single value of 16, and then neglected the modulus mismatch due to the large $\alpha$ value.

The two methods mentioned above both predicted more pronounced solid-solution hardening in NiFe and NiCoFe than NiCo. However, due to the different methods used to calculate the atomic-level mismatch, they also provided conflicting predictions. To understand the nanoindentation results and to examine the two methods used for the Labusch model, we used both methods to evaluate the solid solution hardening in NiCo, NiFe, NiCoFe, NiCoCr, and NiFe-20Cr. The results are normalized to the strengthening value from Ni to NiCo for two reasons: 1) to eliminate the effects of different constants (e.g. $f$ in Eq. (7)) used in different references, and 2) nanoindentation hardness values are rarely directly converted to yield strength values for various reasons (e.g. size effect), although they usually have an approximately linear relationship [34].

Fig. 4 indicates that the predictions based on the interatomic spacing matrix method qualitatively agree well with the experimental nanoindentation hardnesses. However, the predictions based on the "effective" atomic size derived from the experimental alloy lattice parameters and Vegard's law cannot correctly account for the higher

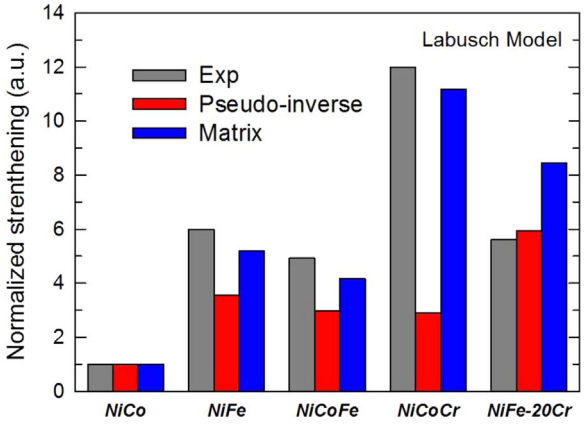


**Fig. 4.** Solid-solution strengthening (normalized to NiCo) from nanoindentation hardness (Exp), the Labusch model prediction, assuming $\alpha = 16$, based on pseudo-inverse analysis (Pseudo-inverse, Ref. [31]), and an interatomic spacing matrix (Matrix, Ref. [32]). In all the three cases, the value of NiCo is defined as 1.

strengthening found in NiCoCr versus NiFe, NiCoFe and NiFe-20Cr.

One of the major sources of such discrepancies is the different interatomic distance (or atomic size) used in the two methods. In the ISM method, the interatomic distance (converted to FCC) of elemental Cr is greater than that of Fe (both greater than Ni and Co), due to the greater experimental lattice parameter of elemental Cr. This assumption leads to a greater lattice mismatch in NiCoCr than in NiCoFe after the matrix calculation, which brings stronger solid-solution strengthening according to the Labusch model. However, experiments (both X-ray and neutron diffractions [35]) have shown that the lattice parameter of NiCoFe is actually greater than that of NiCoCr, opposite to the predictions from the ISM method. Since the PIA method assumes Vegard's law and uses the experimental values of the alloys to derive the effective elemental atomic size, the derived atomic size of Fe is then greater than Cr [31], giving a greater lattice mismatch in NiCoFe than in NiCoCr, which ultimately leads to more strengthening in NiCoFe. On the other hand, due to the magnetostriction effects (e.g. Invar for Ni-65Fe [36]), Ni-Fe alloys show significantly low moduli (e.g. 61 GPa for NiFe and 60 GPa for NiCoFe [13]), resulting in a large modulus mismatch between Ni and Fe elements, which is not considered in the methods from Toda-Caraballo et al. Consequently, both lattice and modulus mismatches in Ni-Fe-X alloys are greater than in the Ni-Cr-X alloys derived from the PIA method, which leads to a prediction of strengthening (NiCoFe > NiCoCr) contrary to experimental results. Another recently developed theory [37] that successfully predicted the strengthening of most of these FCC SP-CSAs seems to face a similar issue: the Burgers vectors predicted for NiCoCr and NiCoFeCr are higher than the experimental values, while predictions for the alloys without Cr (e.g. NiCo, NiFe, NiCoFe, etc.) match the experimental values well; the predicted Burgers vector of NiCoCr is greater than that of NiCoFe, while the experiments show a reversed result.

Since it is the “mismatch”, rather than the absolute value, of lattice parameters that determines the strengthening effects, tiny differences in the use of interatomic distance can yield significant error in the strengthening effects. Thus, caution should be used in application of the Labusch model. More fundamental studies, e.g. ab initio methods, are required for optimum application of this model. It seems that the mechanical properties of Ni-containing concentrated solid solution alloys are not solely determined by adding certain elements; rather the combinations are very important.

## 5. Summary and conclusions

Single crystal NiCoFe, NiCoCr, and NiFe-20Cr alloys have been successfully grown. Their monocrystalline elastic constants have been measured using an ultrasonic method. A few key mechanical and thermal dynamic properties (e.g. shear modulus, bulk modulus, Poisson's ratio, elastic anisotropy, and Debye temperatures) have been derived from the elastic constants, and compared well with the values from the polycrystalline samples. Nanoindentation tests on their (100) surfaces have revealed that all the alloys exhibit typical FCC slip traces. To investigate the solid-solution strengthening mechanisms, their nanoindentation hardnesses have been compared with Ni, NiCo, NiFe and each other. NiCoCr has much higher hardness than all the other alloys, while NiFe, NiCoFe and NiFe-20Cr have similar hardnesses, and NiCo has little hardening effect. The Labusch model has been used to understand the hardening effects, with two methods of calculating the lattice mismatch. By using an interatomic spacing matrix method, the hardening predicted by the Labusch model corresponds well with the experimental results. However, by deriving effective elemental atomic spacing from experimental alloy lattice parameters based on Vegard's law, the Labusch model cannot correctly predict the relative hardening effects between certain alloys. Our results show that using the Labusch model to predict solid-solution strengthening requires careful evaluation of the necessary parameters, especially when Vegard's law is used to obtain the effective atomic spacing.

## Acknowledgements

This work was supported by the Department of Energy, Office of Science, Basic Energy Sciences, Materials Sciences and Engineering Division. Work by KJ was performed as part of the Energy Dissipation to Defect Evolution (EDDE), an Energy Frontier Research Center funded by the U.S. Department of Energy, Office of Science, Basic Energy Sciences. We thank Dr. C. M. Silva at ORNL for his help in powder X-ray diffraction. We thank Dr. I. Toda-Caraballo at University of Cambridge for the helpful discussions on the interatomic spacing matrix analysis.

## Appendix A. Supporting information

Supplementary data associated with this article can be found in the online version at doi:10.1016/j.msea.2017.04.003.

## References

[1] B. Cantor, I.T.H. Chang, P. Knight, A.J.B. Vincent, Microstructural development in equiatomic multicomponent alloys, Mater. Sci. Eng. A 375–377 (2004) 213–218.
[2] O.N. Senkov, G.B. Wilks, J.M. Scott, D.B. Miracle, Mechanical properties of $Nb_{25}Mo_{25}Ta_{25}W_{25}$ and $V_{20}Nb_{20}Mo_{20}Ta_{20}W_{20}$ refractory high entropy alloys, Intermetallics 19 (2011) 698–706.
[3] M.S. Lucas, G.B. Wilks, L. Mauger, J.A. Muñoz, O.N. Senkov, E. Michel, J. Horwath, S.L. Semiatin, M.B. Stone, D.L. Abernathy, E. Karapetrova, Absence of long-range chemical ordering in equimolar FeCoCrNi, Appl. Phys. Lett. 100 (2012) 251907.
[4] F. Tancret, I. Toda-Caraballo, E. Menou, P.E.J. Rivera Díaz-Del-Castillo, Designing high entropy alloys employing thermodynamics and Gaussian process statistical analysis, Mater. Des. 115 (2017) 486–497.
[5] B. Gludovatz, A. Hohenwarter, D. Catoor, E.H. Chang, E.P. George, R.O. Ritchie, A fracture-resistant high-entropy alloy for cryogenic applications, Science 345 (2014) 1153–1158.
[6] B. Gludovatz, A. Hohenwarter, K.V. Thurston, H. Bei, Z. Wu, E.P. George, R.O. Ritchie, Exceptional damage-tolerance of a medium-entropy alloy CrCoNi at cryogenic temperatures, Nat. Commun. 7 (2016) 10602.
[7] Y.D. Wu, Y.H. Cai, X.H. Chen, T. Wang, J.J. Si, L. Wang, Y.D. Wang, X.D. Hui, Phase composition and solid solution strengthening effect in TiZrNbMoV high-entropy alloys, Mater. Des. 83 (2015) 651–660.
[8] K. Jin, B.C. Sales, G.M. Stocks, G.D. Samolyuk, M. Daene, W.J. Weber, Y. Zhang, H. Bei, Tailoring the physical properties of Ni-based single-phase equiatomic alloys by modifying the chemical complexity, Sci. Rep. 6 (2016) 20159.
[9] Y. Zhang, G.M. Stocks, K. Jin, C. Lu, H. Bei, B.C. Sales, L. Wang, L.K. Beland, R.E. Stoller, G.D. Samolyuk, M. Caro, A. Caro, W.J. Weber, Influence of chemical disorder on energy dissipation and defect evolution in concentrated solid solution alloys, Nat. Commun. 6 (2015) 8736.
[10] B.C. Sales, K. Jin, H. Bei, G.M. Stocks, G.D. Samolyuk, A.F. May, M.A. McGuire, Quantum critical behavior in a concentrated ternary solid solution, Sci. Rep. 6 (2016) 26179.
[11] K.Y. Tsai, M.H. Tsai, J.W. Yeh, Sluggish diffusion in Co–Cr–Fe–Mn–Ni high-entropy alloys, Acta Mater. 61 (2013) 4887–4897.
[12] Z. Wu, H. Bei, F. Otto, G.M. Pharr, E.P. George, Recovery, recrystallization, grain growth and phase stability of a family of FCC-structured multi-component equiatomic solid solution alloys, Intermetallics 46 (2014) 131–140.
[13] Z. Wu, H. Bei, G.M. Pharr, E.P. George, Temperature dependence of the mechanical properties of equiatomic solid solution alloys with face-centered cubic crystal structures, Acta Mater. 81 (2014) 428–441.
[14] K. Jin, C. Lu, L.M. Wang, J. Qu, W.J. Weber, Y. Zhang, H. Bei, Effects of compositional complexity on the ion-irradiation induced swelling and hardening in Ni-containing equiatomic alloys, Scr. Mater. 119 (2016) 65–70.
[15] C. Lu, L. Niu, N. Chen, K. Jin, T. Yang, P. Xiu, Y. Zhang, F. Gao, H. Bei, S. Shi, M.-R. He, I.M. Robertson, W.J. Weber, L. Wang, Enhancing radiation tolerance by controlling defect mobility and migration pathways in multicomponent single-phase alloys, Nat. Commun. 7 (2016) 13564.
[16] D.B. Miracle, O.N. Senkov, A critical review of high entropy alloys and related concepts, Acta Mater. 122 (2017) 448–511.
[17] F.H. Hayes, M.G. Hetherington, R.D. Longbottom, Thermodynamics of duplex stainless steels, Mater. Sci. Technol. 6 (1990) 263–272.
[18] H. Bei, E.P. George, Microstructures and mechanical properties of a directionally solidified NiAl-Mo eutectic alloy, Acta Mater. 53 (2005) 69–77.
[19] Y.Z. Xia, H. Bei, Y.F. Gao, D. Catoor, E.P. George, Synthesis, characterization, and nanoindentation response of single crystal Fe–Cr–Ni alloys with FCC and BCC structures, Mater. Sci. Eng. A 611 (2014) 177–187.
[20] H.M. Ledbetter, R.P. Reed, Elastic properties of metals and alloys, 1. iron, nickel, and iron-nickel alloys, J. Phys. Chem. Ref. Data 2 (1973) 531–618.
[21] G. Simmons, H. Wang, Single Crystal Elastic Constants and Calculated Aggregate Properties: A Handbook, The M.I.T Press, Cambridge, Massachusetts, and London, England, 1971.
[22] W. Li, Y. Gao, H. Bei, On the correlation between microscopic structural heterogeneity and embrittlement behavior in metallic glasses, Sci. Rep. 5 (2015) 14786.
[23] Z. Wu, Temperature and Alloying Effects on the Mechanical Properties of

Equiatomic FCC Solid Solution Alloys, Ph.D Dissertation in Materials Science and Engineering, Knoxville, 2014.
[24] H.W. King, Quantitative size-factors for metallic solid solutions, J. Mater. Res. 1 (1966) 79–90.
[25] P. Nash, The Cr-Ni (chromium-nickel) system, Bull. Alloy Phase Diagr. 7 (1986) 466–476.
[26] T.H. Hazlett, E.R. Parker, Effect of some solid solution alloying elements on the creep parameters of nickel, Trans. ASM 46 (1954) 701.
[27] A. Teklu, H. Ledbetter, S. Kim, L.A. Boatner, M. McGuire, V. Keppens, Single-crystal elastic constants of Fe-15Ni-15Cr alloy, Metallur. Mater. Trans. A 35 (2004) 3149–3154.
[28] O.L. Anderson, A simplified method for calculating the Debye temperature from elastic constants, J. Phys. Chem. Solids 24 (1963) 909–917.
[29] Rigidity modulus: periodicity, ⟨https://www.webelements. com/periodicity/rigidity_modulus/.WebElements⟩, 2017.
[30] R. Labusch, A statistical theory of solid solution hardening, Phys. Stat. Sol. 41 (1970) 659–669.
[31] Z. Wu, Y. Gao, H. Bei, Thermal activation mechanisms and Labusch-type strengthening analysis for a family of high-entropy and equiatomic solid-solution alloys, Acta Mater. 120 (2016) 108–119.
[32] I. Toda-Caraballo, A general formulation for solid solution hardening effect in multicomponent alloys, Scr. Mater. 127 (2016) 113–117.
[33] H.A. Moreen, R. Tagaart, D.H. Polonis, A model for the prediction of lattice parameters of solid solutions, Metall. Trans. 2 (1971) 265–268.
[34] R. Rodriguez, I. Gutierrez, Correlation between nanoindentation and tensile properties: influence of the indentation size effect, Mater. Sci. Eng. A 361 (2003) 377–384.
[35] K. Jin, S. Mu, K. An, W.D. Porter, G.D. Samolyuk, G.M. Stocks, H. Bei, Thermophysical properties of Ni-containing single-phase concentrated solid solution alloys, Mater. Des. 117 (2017) 185–192.
[36] M. van Schilfgaarde, I.A. Abrikosov, B. Johansson, Origin of the Invar effect in iron–nickel alloys, Nature 400 (1999) 46–49.
[37] C. Varvenne, A. Luque, W.A. Curtin, Theory of strengthening in fcc high entropy alloys, Acta Mater. 118 (2016) 164–176.